Conference on Modelling Fluid Flow (CMFF'22)
The 18th International Conference on Fluid Flow Technologies
Budapest, Hungary, August 30-September 2, 2022

EFFICIENT PIV MEASUREMENTS IN THE INTERIOR OF COMPLEX, TRANSPARENT GEOMETRIES

Mirko EBERT[1], Christin VELTEN[2], Katharina ZÄHRINGER[2], Christian LESSIG[1]

[1] Corresponding Author. Institute for Simulation and Graphics, Department of Computer Science, Otto-von-Guericke-Universität Magdeburg. Universitätsplatz 2, 39106 Magdeburg, Germany. E-mail: {mirko.ebert | christian.lessig}@ovgu.de
[2] Lehrstuhl für Strömungsmechanik und Strömungstechnik, Fakultät für Verfahrens- und Systemtechnik, Otto-von-Guericke-Universität Magdeburg. E-mail: {christin.velten | katharina.zaehringer }@ovgu.de

ABSTRACT

In many industrial applications, such as packed beds and combustion engines, gas flows through complex geometries play an important role. The measurement of these is therefore of considerable importance, e.g. for process monitoring and optimization. Spatially and temporally highly resolved measurements of these flows are, however, often difficult since no direct optical access to the interior is possible, rendering techniques such as PIV inapplicable. Transparent geometry, e.g. from glass, restores optical access but it leads to severe optical distortions in captured images, again preventing the use of standard techniques. We present an efficient and robust numerical algorithm to reconstruct gas flow velocity vector fields in the interior of complex, transparent geometry from PIV measurements. A complete simulation of PIV experiments, which allows, e.g., to optimize an experimental setup without building hardware, is also introduced. We validate our PIV reconstruction technique with simulated experiments as well as real-world PIV measurements in a complex bulk reactor.

Keywords: PIV, ray tracing, flow velocity measurement in transparent packed bed

1. INTRODUCTION

Particle image velocimetry (PIV) is a well established technique to obtain spatially and temporally highly resolved velocity field measurements of gaseous flows [1]. Since PIV is based on imaging the flow, it requires the investigation region to be optically accessible. This, however, is not easily satisfied in many applications where there is complex flow geometry. One example are bulk reactors where immersed particles play a fundamental role for the overall dynamics but these also block the line of sight to many flow regions of interest.

In this article, we present an efficient and robust numerical technique for PIV-based flow velocity measurements in complex environments. We assume that geometries that would block the line of sight are of transparent material, e.g. glass. This ascertains optical access but also causes strong optical distortions in captured PIV images, rendering standard PIV calculation techniques inapplicable. In our work, we resolve this by numerically computing the undistorted PIV image that would have been obtained for the flow with its tracer particles in a geometry that has no optical effect.

We obtain the undistorted image with a two step technique. First, we reconstruct the light field, which describes the light energy density as a function of position and direction, on the PIV investigation plane. This is accomplished using an inverse light transport simulation of a computer model of the experimental setup that uses the distorted PIV image as light source. With the light field available, a forward optical simulation in an empty environment yields the undistorted PIV image, which can be used with standard PIV vector field calculation techniques. Our approach is nontrivial since the problem is a priori ill-posed and we discuss how it can, nonetheless, robustly yield corrected images and high fidelity vector fields.

We demonstrate the efficacy of our technique using, firstly, simulated PIV experiments, in which case the ground truth vector field is precisely known, and, secondly, real PIV experiments in a complex bulk reactor. We also investigate how regions where no vector field reconstruction is possible can be minimized with multi-camera PIV setups.

The remainder of the article is structured as follows. After discussing related work in Sec. 1, we present in Sec. 2 our numerical technique to enable PIV in optically complex environments. In Sec. 3 we verify our technique with simulated PIV experiments and in Sec. 4 we present results for real ones in a bulk reactor. The paper concludes in Sec. 5 where we also discuss future work.

Related Work The measurement of flow fields in complex geometries is challenging since optical methods, such as PIV or PTV (particle tracking velocimetry), are not directly applicable. Using transparent geometry, e.g. of glass, restores optical access. However, it also induces strong optical distortions, for example due to strongly curved or angled transparent surfaces, which render standard techniques for flow field calculation inapplicable.

In liquids, refractive index matching (RIM), where the refractive index of the flow liquid is matched to that of the immersed, transparent geometry, can be employed to counterbalance the distortion. This was used in conjunction with optical methods to compute flow vector fields in packed beds for example in [2, 3, 4, 5]. In gaseous flows, however, RIM is inapplicable due to the large difference between refractive indices.

Invasive techniques, such as endoscopic PIV, provide an alternative approach for flow measurements when optical access from the outside is not possible. This was used, for example, to analyze velocity fields of water flows in the porous space of packed beds [6, 7]. The insertion of probes into a flow can, however, have a significant effect on its behavior.

For simple optical setups, e.g. when the experimental apparatus is viewed through a slightly curved window, optical distortions can be corrected for by careful calibration [8, 9]. Kováts et al. [10] demonstrated that this is still applicable in more challenging configurations with a single layer of hollow spheres. These authors used multi-step calibration with the interstices and the spheres being considered separately.

For large optical distortions, more sophisticated methods than careful calibration are required. Kang et al. [11] developed a correction for the flow field inside a droplet using ray tracing. Some terms in their algorithm were found to be erroneous by Minor et al. [12] who corrected these. Later, Zha et al. [13] used ray tracing for distortion correction of flow measurements in a transparent diesel motor cylinder.

For complex particle beds, the use of ray tracing to correct for optical distortions was first demonstrated by Martins et al. [14, 15]. We will spell out the implicit assumptions in this work, extend it to scale better to more complex setups, and allow for the recovery of larger areas of the flow fields.

2. PIV IN OPTICALLY COMPLEX ENVIRONMENTS

We consider PIV setups with complex geometry that is transparent at least in the line of sight of the measurement camera. Optical access to the flow is then still available but the transparent geometry causes strong distortions in captured PIV images that lead to incorrectly computed vector fields when standard techniques for PIV vector field calculation are used; see the experimental results in Fig. 6. Our approach to obtain the true vector fields is to reconstruct the light field $\ell(x, \omega)$ on the PIV investigation plane and then simulate the image formation process as if no distorting geometry would be present, see Fig. 1 for an overview. This yields a corrected PIV image that can be used with standard approaches for PIV vector field calculations.

Although the light field $\ell(x, \omega)$ can in principle be obtained by tracing the measured light intensity $I(u)$ from the PIV images back through the experimental setup, the computation is ill-posed since the measurement on the camera reduces the $5D$ function $\ell(x, \omega)$ that depends on position x and direction ω to the $2D$ intensity $I(u)$, averaging the contributions coming from different directions and projecting it onto the two-dimensional image plane.[1] The reconstruction is furthermore compounded by the need for a minute alignment between experiment and simulation as well as magnification effects that can cause the projection of large regions of the PIV investigation plane onto a small number of pixels.

In the following, we will detail our numerical technique that, despite the difficulties, allows for the computation of corrected PIV images and, through this, the accurate calculation of vector fields with PIV in optically complex environments. We will first consider the light field reconstruction and then the alignment between experiment and simulation.

2.1. Light field reconstruction

To obtain a corrected PIV image that allows for the use of standard PIV software, we require knowledge of the light field $\ell(x, \omega)$ on the investigation plane P at the time when the image is taken. The available information for the reconstruction is, however, only the distorted PIV measurement, i.e. the two-dimensional intensity function $I(u) : \mathcal{I} \to \mathbb{R}$ on the image plane $\mathcal{I}$. A reconstruction is, therefore, only possible when additional assumptions about the light field are made.

We will assume, firstly, that the distorted PIV image was captured with a pinhole camera model so that the contributions to $I(u)$ for fixed $u \in \mathcal{I}$ come from a single direction only and, secondly, that the light field $\ell(x, \omega)|_P$ on the PIV investigation plane is isotropic and has no angular dependence, i.e. $\ell(p) = \ell(x, \omega)|_P$ with $p \in P$.

The pinhole camera, with focal length and lens distortion as parameters, is fitted to best match the real camera in the experiment, see Sec. 2.2 for details. This provides a good approximation, as is corroborated by Fig. 2 that shows a pixel-accurate agreement between the geometries in a photograph and a computer-generated image with the fitted pinhole camera.

An isotropic light field ignores the strong anisotropy in the Mie scattering of the tracer particles.

[1] By the symmetry of the light field, which corresponds to the constancy of $\ell(x, \omega)$ along light rays, the function is, in fact, only four-dimensional; the reconstruction problem remains, however, ill-posed.

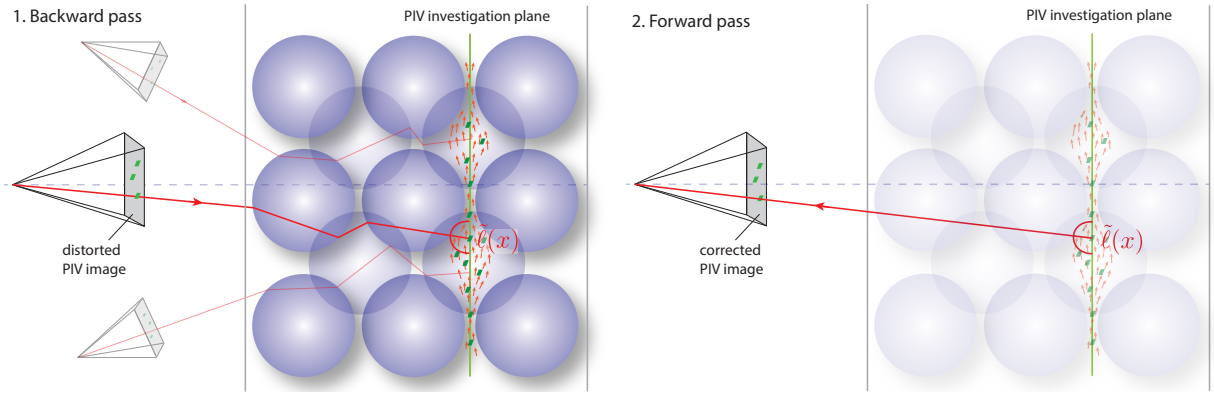

Figure 1. Conceptual depiction of our reconstruction algorithm with spheres as transparent flow geometry. In the forward pass, the captured PIV image is used as a light source and with a ray tracing light transport simulation through the experimental setup, an approximation $\tilde{\ell}(x) = \tilde{\ell}(x, \omega)$ of the light field on the PIV investigation plane is reconstructed. The use of multiple PIV cameras is also possible and this can lead to improved reconstructions of $\tilde{\ell}(x)$. After the reconstruction of $\tilde{\ell}(x)$, the undistorted PIV image is reconstructed by forward ray tracing with $\tilde{\ell}(x)$ as light source and with the distorting geometry removed from the experimental setup, which is easily realized numerically. Standard PIV software can then be used to compute the flow vector field.

This effect is nevertheless considerably reduced in a camera arrangement, where the scattered light is collected over a range of angles, depending on the distance (which is rather large in our case) and aperture of the camera, as well as in a field of particles where multi-scattering takes place [1]. Furthermore, what is used for the velocity field determination is, however, only the relative position of tracer particles in an image pair, with the magnitude Fourier-averaged over an interrogation window. In this sense the assumption of an isotropic light field can be understood as an analogue of the binarization that is sometimes performed as image pre-processing before PIV. In more complex camera setups, e.g. those considered in Sec. 3.1, an anisotropic light field might be beneficial or necessary. This will be the subject of future work.

With the above assumptions, the mapping of the $2D$ function $I(u)$ to the $2D$ function $\ell(p)$ is well posed. In particular, an approximation $\tilde{\ell}(p)$ to $\ell(p)$ can be obtained by tracing light rays backwards from the camera with the distorted PIV image as source until the rays intersect P, see Fig. 1, left. By the reversibility of light transport, pointwise values $\ell(p)$ are obtained by reflecting and refracting the rays through the scene and scattering these according to the Fresnel equations [16]. We record all $\ell(p)$ which, when interpolated, provide the approximation $\tilde{\ell}_P$. The corrected PIV image I_c, which allows for the use of standard PIV calculations for determining the flow velocity field, is then obtained by simulating the image formation process for an experimental setup with $\tilde{\ell}(x)$ as light source and with all distorting geometry removed, see Fig. 1, right.

It is possible to consider the above computation as a mapping $M : I \to I_c$ from the distorted PIV image I to the corrected one I_c, side-stepping an explicit computation of $\tilde{\ell}$. This was followed in [14, 15]. However, the approach scales quadratically in the number of pixels, so that for state-of-the-art camera resolutions with $O(10^7)$ or more pixels, the mapping M requires tens of gigabytes of storage. Furthermore, since on modern compute hardware the bottleneck is usually memory transfer and not computations, performing the ray tracing for every image that is to be reconstructed is in practice faster than applying a precomputed mapping.

2.2. Alignment of Experimental Setup and Simulation

A precise alignment between simulation and experiment is critical for an accurate correction of distorted images. We thereby currently presume that an accurate 3D model of the experimental setup exists, e.g. because it served as input to its manufacturing, so that the alignment reduces to calibrating the camera. Following the approach in computer vision [17], we separate this calibration into an intrinsic part, which determines the camera parameters that best match a pinhole camera model and which corrects for lens distortion, and an extrinsic one, which accounts for the rigid alignment of the camera with respect to the experimental setup. Among other things, this separation has the advantage that different numerical techniques can be used for the different parts, which we exploit in our approach. Both calibrations are performed in the experimental setup prior to the flow measurement.

For the intrinsic calibration, we experimented with the OpenCV library [18] as well as with the commercial PIV software DaVis from LaVision. We obtained the best results with a combination of both when the focal length and the optical center are determined with the DaVis calibration and the lens dis-

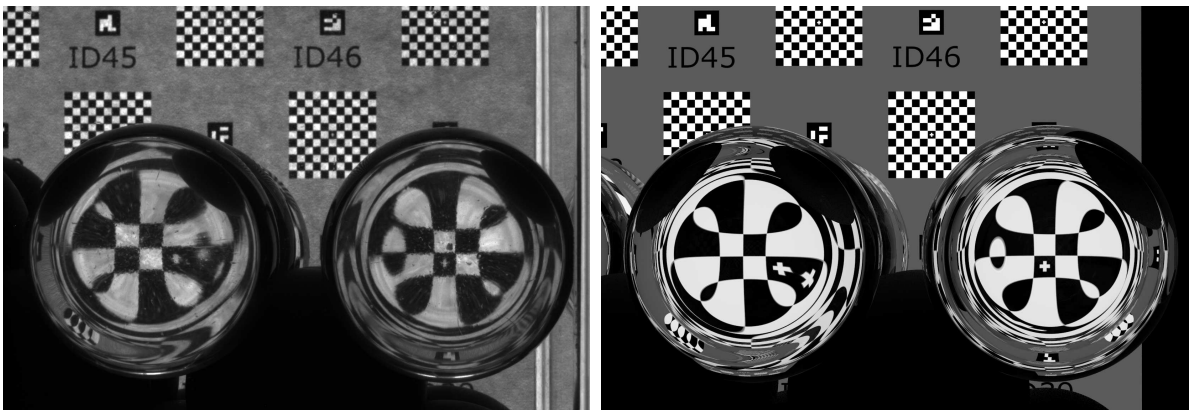

Figure 2. Comparison between photograph of an experimental setup without a flow (left) and computer-generated image of it (right). A good agreement with a pixel-accurate alignment of the geometry can be observed.

tortion subsequently in OpenCV.

For extrinsic calibration, we use AruCo markers that integrated into the experimental setup (cf. Fig. 2) so that we have always a sufficient number of markers in the field of vision. The markers consist of a barcode that allows for their unique identification and they are placed at non-colinear, known positions in the experimental setup, see Fig. 2. Using a geometric description of the relative marker positions, standard libraries, e.g. [18], can be used to obtain an estimation of the camera position relative to these. For us, this provides the position of the camera and its orientation with respect to the experimental setup. The camera's position would also be available from the setup itself, at least up to measurement uncertainties, but not the orientation, which is critical for an accurate reconstruction [14].

To verify the accuracy of the calibration we compare for each experimental run a computer-generated image of the corresponding experimental setup with a photograph, both without flow to facilitate the comparison. An example is shown in Fig. 2. As can be seen there, a good agreement is achieved and an overlay of the images verifies that one has a pixel-accurate alignment of the geometry. An even closer match of the images could be obtained by also simulating depth-of-field but since this does not facilitate PIV reconstruction we do not perform the expensive additional computations. Fig. 2 also shows that for our concrete setup the computer model is sufficiently accurate for the light transport simulation. However, at least locally a strong sensitivity to errors in the computer model exists for both the geometry and parameters such as the refractive index. A quantitative analysis of the sensitivity will be pursued in future work.

2.3. Implementation

Our implementation of the light transport simulation is based on the open source ray tracing software pbrt [19], which provides a flexible and efficient Monte Carlo light transport simulator designed for research. Some modifications to the software were necessary to adapt it for our purposes. The most important ones are a textured area light source, which is used for the captured PIV image; an implementation of a pinhole camera with lens distortion, which matches the model of OpenCV; a surface material that represents the reconstructed light field in the scene; and extending the light ray representation in the software so that it has information about the ray's origin and destination. In our implementation, we also do not explicitly record $\tilde{\ell}$ but exploit that the forward pass (cf. Fig. 1) is very simple and allows one to directly compute the corrected image I_c. For an experimental setup with 12 visible spheres, the computation time of I_c from a given distorted PIV image I at a resolution of 1000×1000 pixels is 6.5 s on a 12 core processor with 2.2 GHz.

The pbrt-based implementation of the light transport simulation is complemented by python code for the calibration as well as the necessary data conversion between the different parts of the processing pipeline.

3. SIMULATED PIV EXPERIMENTS

In this section, we consider the validation of the computational pipeline introduced in Sec. 2 with simulated PIV experiments to obtain insight on the influence of different parameters, like geometric tolerances and camera orientation and position. While the present work provides only first steps in this direction, it will in the future help with the design and and planning of experiments. This allows us to compare to a known ground truth and also to control and separate different error sources. In Sec. 3.1 we detail the principle methodology for this and in Sec. 3.2 the concrete realization as well as the obtained results are discussed. We also demonstrate that simulated PIV experiments can help to minimize difficulties in the experiments and reconstructions, which is considerably more efficient when done numerically than with real experiments.

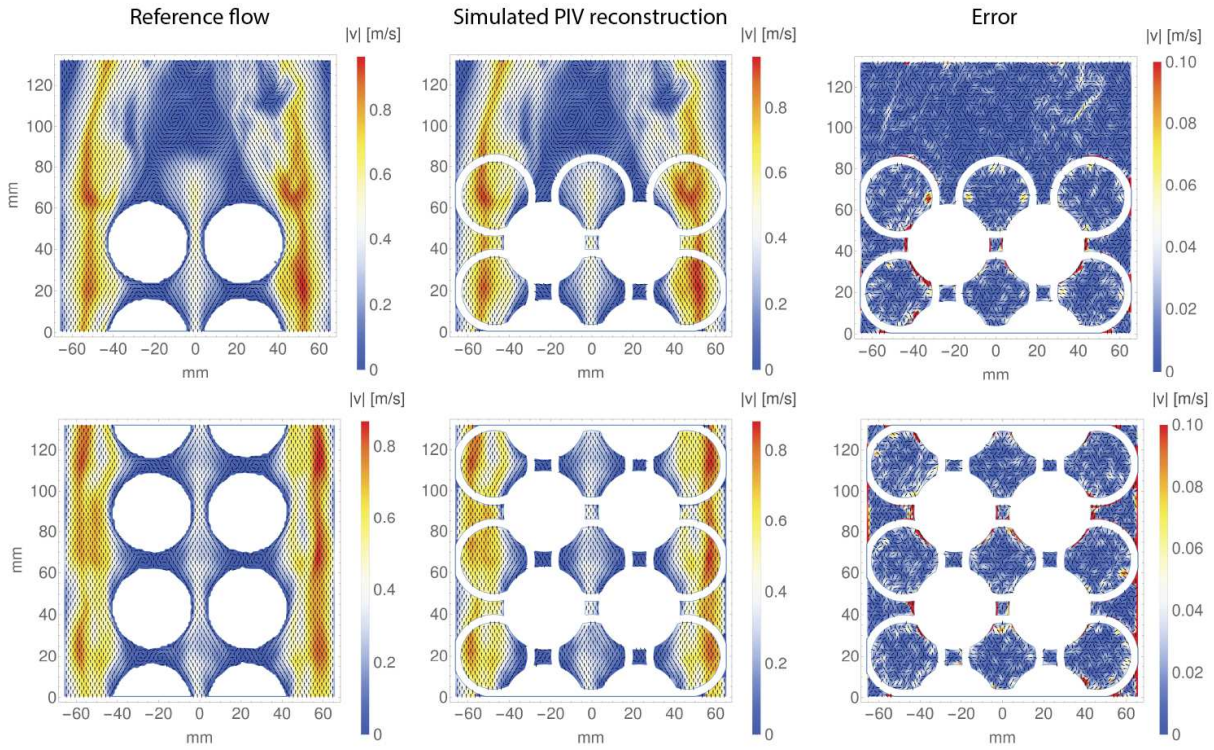

Figure 3. CDF simulated reference (left), calculated flow vector fields (center), and difference (right) for the top layer (top) and eleventh layer (bottom) of the packing in the bulk reactor in Fig. 4. In each case, the virtual PIV investigation plane was horizontally behind two layers of spheres of the 3×3 layout and thus cut through the spheres of the subjacent layer, resulting in the circular regions where even in the reference no vector field is defined. The error is the difference between the reference and the computed vector field.

3.1. Simulation of PIV experiments

The input for the simulated PIV experiments is a 3D computer model of the experimental setup as well as a simulation of the flow through it. Trajectories of PIV tracer particles along the flow are obtained by integrating the fluid vector field numerically from random but well distributed initial conditions for the time between the two PIV images (e.g. 10^{-4} s). The particles at their start and end positions are stored in images that represent the laser sheet of the PIV investigation plane at the two different times, with particle sizes chosen to be optimal for PIV evaluation. The images corresponding to the PIV laser sheet are subsequently used as light source for a light transport simulation through the computer model of the experimental setup (with the full geometry) to determine the distorted PIV images that would have been captured by a measurement camera.

After the distorted PIV images have been obtained, the computations proceed as described in Sec. 2 to reconstruct corrected images.

3.2. Validation

For validation, we used a preliminary computer model of the bulk reactor in the experiments of Sec. 4, shown in Fig. 4, with a flow simulation in it performed with the Lattice-Boltzmann code ALBORZ [20]. For time integration of virtual PIV tracer particles, the classical Runge-Kutta-4 scheme was employed. We currently use a pinhole camera to capture simulated PIV images, although more complex and realistic models are possible [21]. Vector fields were calculated from corrected, simulated PIV images using the commercial PIV software DaVis from LaVision. Since all geometric parameters are exactly known, no alignment between (virtual) experiment and simulation, as described in Sec. 2.2, was necessary.

Calculated flow vector fields for two different measurement positions in the bulk reactor (surface on top and eleventh layer on bottom) are shown in Fig. 3, center, and the reference flow field from the simulation in Fig. 3, left. Minor artifacts, for example in the interstices between the particles where fine vortical structures are not fully resolved, can be observed by comparing both columns. Overall, however, an accurate reconstruction of the flow field is obtained.

In the right column of Fig. 3, the differences between reference flow field and simulated PIV are depicted. The white circular regions in Fig. 3 result from very strong optical distortions at the rim of the spheres in front of the measurement plane. Through the distortion, the corresponding regions on the PIV investigation plane are mapped onto a single or a small number of pixels on the camera image, rendering reconstruction impossible. Therefore, the regions

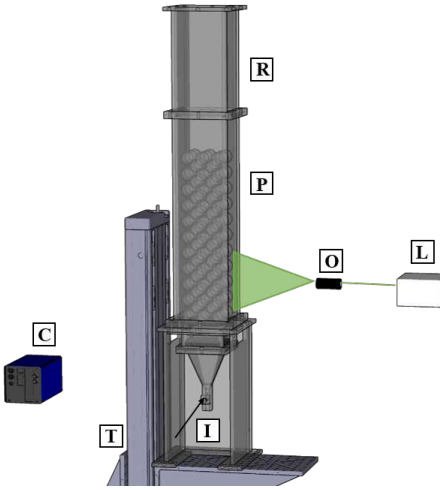

Figure 4. Experimental Setup consisting of a bulk reactor (R), the bcc-packing (P), the air inlet (I), the laser Quantel Q-smart Twins 850 (L), the camera (C), the light sheet optics (O) and a 3D-traversing system (T).

are masked for PIV vector field calculations to avoid that the distortions affect larger neighborhoods.

PIV vector field calculations from the simulated experiments and with ray tracing corrected particle images lead to an average uncertainty of $2.211 \cdot 10^{-5}$ m/s. This demonstrates that very few errors are introduced by the simulation and correction method. The good results are partially a consequence of the lack of imperfections and misalignments that are unavoidable in real-world experiments. However, in our opinion, this demonstrates an advantage of the simulation since the different components of a real setup can be studied independently and the errors introduced by these can be delineated (for the components and effects that are present in the necessarily simplified simulation). In particular, the integration of, for example, an imperfect camera or alignment errors into the simulation is easily possible.

3.3. Reduction of Non-Reconstructable Regions

In this section, we use the PIV simulation to investigate how to minimize regions where vector field reconstruction is impossible due to a very large optical distortion, see the rings in Fig. 3 as well as the discussion above. Simulated PIV experiments provide here the advantage that alternatives can be explored significantly more efficiently than with a physical experimental setup.

To minimize non-reconstructable regions, we consider the use of multiple cameras for the PIV measurement. The setup is analogous to that in Fig. 4 but with five synchronized cameras, three of which are in the same plane as the original one and two in an elevated position, see Fig. 1. We compute virtual PIV measurement through these cameras analogous to Sec. 3.1 by performing a light transport simulation for each of them, yielding five simulated PIV images. For the reconstruction of the isotropic light field $\tilde{\ell}(p)$ on the investigation plane, we can now utilize the five PIV measurements and this provides the principal advantage of the multi-camera setup. In particular, each of the five images is used as source for a backward light transport pass as described in Sec. 2.1 and the contributions from the different cameras are accumulated into $\tilde{\ell}(p)$, yielding a more accurate approximation to the original light field $\ell(p)$. This is demonstrated in Fig. 5 for the first configuration in Fig. 3, which corresponds to the surface layer of the packing in the bulk reactor. The regions where no reconstruction was possible previously are completely removed. Some additional artifacts appear in the calculated vector fields that result from multiple reflections and induced poor optical quality in the corrected PIV image. A weighted combination of the different cameras in a multi-camera setup, which will likely allow one to remove the artifacts, will be investigated in future work.

4. PHYSICAL PIV EXPERIMENTS

Next to the simulated PIV experiments presented in the last section, we evaluated our reconstruction algorithm also with preliminary real experiments with a physical realization of the bulk reactor also used in the simulations.

4.1. Experimental Setup

The experimental setup is shown in Fig. 4. A bulk reactor (R) holds a packing of body centered cubic d = 40 mm polypropylene precision spheres and N-BK7 ball lenses (P), which are used in the measurement regions to generate optical access. In the first layer 3×3 spheres are arranged. By moving the reactor, which is placed on a 3D traversing unit (T), the required measurement position and alignment can be generated with the help of a ray tracing calibration target, which is placed on the rear side of the reactor. The measurement plane is created by a light sheet optic (O) and a Quantel Q-smart Twins 850 laser (L). For detection of the measurement signal, coming from illuminated liquid Di-Ethyl-Hexyl-Sebacat (DEHS) tracer particles, an Imager LX 8M Camera (C) from LaVision is used. The tracer particles enter together with the pressurized air controlled by a Bronkhorst Mass-Stream Controller (D-6371) through the reactor inlet (I). Particle fields are recorded with a frequency of $f = 1.67$ Hz. Before the correction is computed as described in Sec. 2, a calibration is applied to the images with the commercial software DaVis from LaVision. The software is also used for vector field calculation from the distortion-corrected images.

4.2. Vector Field Calculation

In this experiment, surface measurements above nine layers of spheres are carried out. The measurement plane is in the centre between the second and third sphere in the camera viewing direction. The

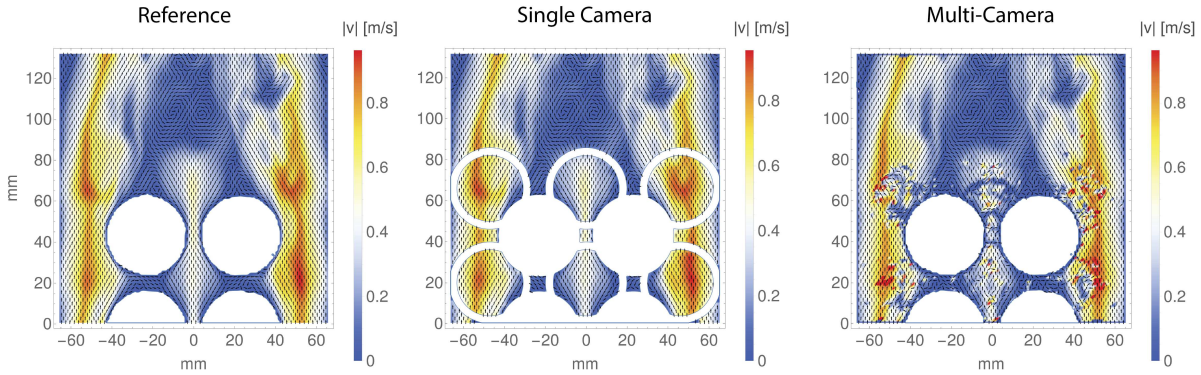

Figure 5. CFD simulated reference flow field (left), and reconstructed vector fields (center and right) for the surface of the packing in the bulk reactor of Fig. 4. In the center is the result for a PIV setup with one camera, which yields circular regions that cannot be reconstructed due to very large optical distortions. In the five camera setup on the right a reconstruction of these regions is possible, although some additional artifacts appear.

flow field of the surrounding can be calculated easily by direct application of standard PIV evaluation with a cross-correlation method, with multi-pass calculation and a decreasing size of the interrogation window from 64×64 to 32×32 pixels with 50% overlap. This leads to the vector fields shown in Fig. 6, top row, for particle Reynolds number $\mathrm{Re_P} = 200$ and $\mathrm{Re_P} = 300$ without (first and third column) and with (second and fourth column) ray tracing based correction. The particle Reynolds number is based on the sphere diameter and a theoretical porosity of a bcc-packing of $\phi = 0.32$.

Even without correction (first and third column) a vector field can be calculated in the distorted region behind the center sphere, although it is corrupted by effects like mirroring and magnification. Due to these and the shadows of the underlying layer of spheres blocking the light sheet, no measurement signal is obtained in the lower region behind the spheres. To obtain the real velocity field, the ray tracing based correction is applied and the resulting images are afterwards evaluated by the same standard PIV calculation as presented above.

After the correction (second and fourth column) the surrounding flow field matches very well the flow behind the centre sphere, where optical distortions were maximal. Directly above the center sphere a region with higher velocities appears, leading to a recirculation zone. Considering the higher velocities in the centre and lower velocities closer to the rim regions of the sphere, the flow fields behind the outer spheres match this condition very well. Unfortunately, the rim region of the spheres cannot be reconstructed completely due to high optical distortions, cf. Sec. 3, leading to the masked white half ring.

The averaged relative uncertainties based on the averaged uncertainty from the uncertainty fields shown in the lower row of Fig. 7 divided by the averaged velocity from the absolute velocity fields are in the range of 2.3% to 3.6%. The presentation of relative uncertainty fields is not practical because of the recirculation zones in the centre of the field, leading to unreasonable high relative uncertainties by division of velocities close to 0 m/s. Comparing the uncertainty fields of the distorted and the corrected data shows no significant difference since only the uncertainty of the PIV evaluation itself is considered by this method. The error of the correction method can only be determined properly by the use of known synthetic reference data, like presented before.

5. CONCLUSION AND FUTURE WORK

In this work, we presented a computationally efficient numerical technique to perform PIV in complex environments with transparent geometry. We validated the technique with simulated PIV experiments, where we obtained good agreement with the known ground truth solutions, and with real experiments in a complex bulk reactor, where high quality velocity fields were obtained. We also demonstrated that simulated PIV experiments are of utility in their own right by using it to investigate how multiple cameras can improve reconstructions.

Next to work on the real experiments with the bulk reactor in Fig. 4, we want to extend our numerical technique into multiple directions. We want to use our simulated PIV experiments to better understand the different sources of errors that occur in physical experiments and devise strategies to minimize these. For this, we also want to use more complex camera models [21]. The principle challenge there is to develop a camera calibration that can robustly account for the additional parameters. Numerical optimization of the computer model to better match the physical experimental setup could also help to improve our technique. Another important direction for future work is a sensitivity analysis of our approach, in particular with respect to errors in the computer model as well as the calibration.

We also want to extend our preliminary results on multi-camera PIV. Importantly, the artifacts that

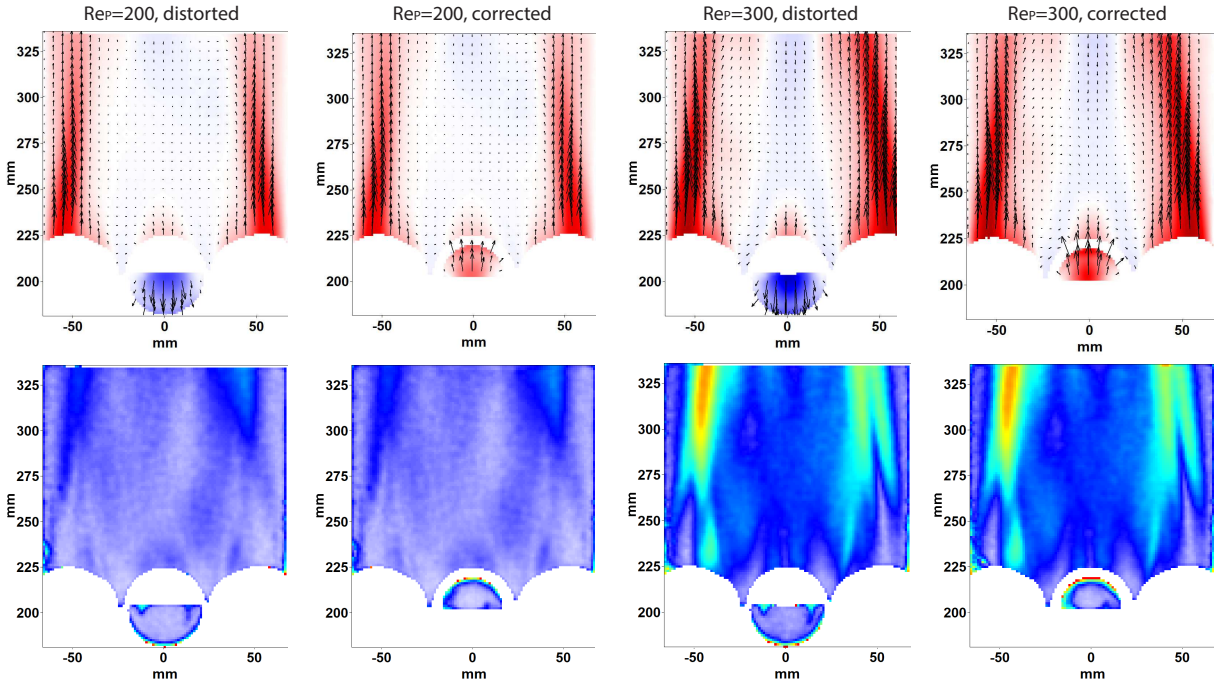

Figure 6. Averaged vertical velocity component V_y as color gradient and entire vector field as overlay for particle Reynolds numbers 200 and 300 above nine layers of spheres calculated by distorted and corrected images (top row) and PIV uncertainty fields below.

are currently visible need to be reduced or avoided. This will likely be possible by appropriately weighting the contributions from different cameras. Interesting is thereby how many cameras are needed and if a sophisticated reconstruction procedure can potentially reduce the number of cameras to not unduly increase the experimental work. The use of multiple cameras also allows one to compute an approximation $\tilde{\ell}(x, \omega)$ to the light field on the PIV investigation plane with angular dependence and we want to investigate if this improves vector field reconstruction. A related direction is the use of a plenoptic camera instead of multiple separate ones. This could increase reconstruction quality and also avoid the considerable challenge that calibration of multiple individual cameras poses in real experiments.

In the future, we also want to publicly release our computational pipeline, including integrations into standard CAD and modeling software.

ACKNOWLEDGEMENTS

Funded by the Deutsche Forschungsgemeinschaft (DFG, German Research Foundation) – Project-ID 422037413 – TRR 287. We thank Ali Husseini and Feng Huang for the the ALBORZ simulation through the bulk reactor that was used in Sec. 3.

REFERENCES

[1] Raffel, M., Willert, C., Scarano, F., Kähler, C. J., Wereley, S. T., and Kompenhans, J., 2018, *Particle Image Velocimetry - A Practical Guide*, Vol. 1, Springer Verlag, URL `https://elib.dlr.de/119724/`.

[2] Budwig, R., 1994, "Refractive index matching methods for liquid flow investigations", *Experiments in Fluids*, Vol. 17 (5), pp. 350–355.

[3] Hassan, Y. A., and Dominguez-Ontiveros, E., 2008, "Flow visualization in a pebble bed reactor experiment using PIV and refractive index matching techniques", *Nuclear Engineering and Design*, Vol. 238 (11), pp. 3080–3085.

[4] Wiederseiner, S., Andreini, N., Epely-Chauvin, G., and Ancey, C., 2010, "Refractive-index and density matching in concentrated particle suspensions: a review", *Experiments in Fluids*, Vol. 50 (5), pp. 1183–1206.

[5] Borrero-Echeverry, D., and Morrison, B. C. A., 2016, "Aqueous ammonium thiocyanate solutions as refractive index-matching fluids with low density and viscosity", *Experiments in Fluids*, Vol. 57 (7).

[6] Tani, N., Kondo, H., Mori, M., Hishida, K., and Maeda, M., 2002, "Development of fiberscope PIV system by controlling diode laser illumination", *Experiments in Fluids*, Vol. 33 (6), pp. 752–758.

[7] Blois, G., Smith, G. H. S., Best, J. L., Hardy, R. J., and Lead, J. R., 2011, "Quantifying the dynamics of flow within a permeable bed using time-resolved endoscopic particle imaging velocimetry (EPIV)", *Experiments in Fluids*, Vol. 53 (1), pp. 51–76.

[8] Willert, C., 1997, “Stereoscopic digital particle image velocimetry for application in wind tunnel flows”, *Measurement Science and Technology*, Vol. 8 (12), pp. 1465–1479.

[9] Soloff, S. M., Adrian, R. J., and Liu, Z.-C., 1997, “Distortion compensation for generalized stereoscopic particle image velocimetry”, *Measurement Science and Technology*, Vol. 8 (12), pp. 1441–1454.

[10] Kováts, P., Thévenin, D., and Zähringer, K., “Experimentelle Untersuchung von Strömungsfeldern in den Zwischenräumen grober Schüttungen”, .

[11] Kang, K. H., Lee, S. J., Lee, C. M., and Kang, I. S., 2004, “Quantitative visualization of flow inside an evaporating droplet using the ray tracing method”, *Measurement Science and Technology*, Vol. 15 (6), pp. 1104–1112.

[12] Minor, G., Oshkai, P., and Djilali, N., 2007, “Optical distortion correction for liquid droplet visualization using the ray tracing method: further considerations”, *Measurement Science and Technology*, Vol. 18 (11), pp. L23–L28.

[13] Zha, K., Busch, S., Park, C., and Miles, P. C., 2016, “A novel method for correction of temporally- and spatially-variant optical distortion in planar particle image velocimetry”, *Measurement Science and Technology*, Vol. 27 (8), p. 085201.

[14] Martins, F. J. W. A., da Silva, C. C., Lessig, C., and Zähringer, K., 2018, “Ray-Tracing Based Image Correction of Optical Distortion for PIV Measurements in Packed Beds”, *JAOP: Journal of Advanced Optics and Photonics*, Vol. 1 (2), pp. 71–94, URL `http://www.techscience.com/doi/10.3970/jaop.2018.903.870.html`.

[15] Martins, F. J. W. A., da Silva, A. C., Lessig, C., and Zähringer, K., 2018, “Ray-Tracing Based Image Correction of Optical Distortions Caused by Transparent Spheres for Application in PIV”, *19th International Symposium on the Application of Laser and Imaging Techniques to Fluid Mechanics*, Lisbon.

[16] Born, M., and Wolf, E., 1999, *Principles of Optics: Electromagnetic Theory of Propagation, Interference and Diffraction of Light*, Cambridge University Press, Cambridge, seventh edn.

[17] Hartley, R., and Zisserman, A., 2003, *Multiple View Geometry in Computer Vision*, Cambridge University Press, New York, NY, USA, 2 edn., ISBN 0521540518.

[18] Bradski, G., 2000, “OpenCV”, *Dr Dobb’s Journal of Software Tools*.

[19] Pharr, M., and Humphreys, G., 2010, *Physically Based Rendering: From Theory to Implementation*, Morgan Kaufmann Publishers Inc., San Francisco, CA, USA, second edn.

[20] Hosseini, S. A., 2020, “Development of a lattice Boltzmann-based numerical method for the simulation of reacting flows”, Ph.D. thesis, université Paris-Saclay.

[21] Kolb, C., Mitchell, D., and Hanrahan, P., 1995, “A Realistic Camera Model for Computer Graphics”, *Proceedings of SIGGRAPH ’95*, ACM Press, New York, New York, USA, ISBN 0897917014, pp. 317–324, URL `http://portal.acm.org/citation.cfm?id=218380.218463`.